

Exploring microstructural changes associated with oxidation in Ni–YSZ SOFC electrodes using high resolution X-ray computed tomography

P.R. Shearing^{a,*}, R.S. Bradley^c, J. Gelb^d, F. Tariq^b, P.J. Withers^c, N.P. Brandon^b

^a Dept. Chemical Engineering, University College London, WC1E 7JE, UK

^b Dept. Earth Science and Engineering, Imperial College London, SW7 2AZ, UK

^c Henry Moseley X-ray Imaging Facility, School of Materials, University of Manchester, M1 7HS, UK

^d Xradia Inc, Pleasanton, CA 94588, USA

ARTICLE INFO

Article history:

Received 1 July 2011

Received in revised form 29 September 2011

Accepted 17 October 2011

Available online 26 November 2011

Keywords:

SOFC microstructure

Redox cycling

X-ray nano-CT

4D tomography

ABSTRACT

State of the art solid oxide fuel cell (SOFC) anodes are typically Ni based, one of the primary drawbacks of these electrodes is their significant dimensional change upon oxidation. As commercial SOFCs may typically be expected to undergo numerous redox cycles in their operating lifetime, it is important to understand the associated microstructural degradation process. Here we present a methodology for the use of synchrotron based X-ray nano-computed tomography to explore the step-wise oxidation of the Ni phase in a Ni–YSZ composite material. This non-destructive technique demonstrates the potential to track microstructural evolution on a grain-by-grain basis in three dimensions.

© 2011 Elsevier B.V. All rights reserved.

1. Introduction

In state of the art solid oxide fuel cells (SOFCs) the reactions are supported by porous composite electrodes, providing intimate contact of an electronic, ionic and pore phase at triple phase boundary points distributed normal to the electrode–electrolyte interface. The length and distribution of these triple phase boundary points are widely thought to directly dictate the catalytic performance of the electrodes; however electrode microstructure has many roles affecting operation in ohmic and mass-transport dominated regimes. In electrode-supported designs, the anode may also be expected to fulfill an additional requirement as a structural support.

Ni mixed with an ionic conducting phase (CGO or YSZ) is a common choice for anode material owing to its cost and excellent catalytic activity for hydrogen oxidation. However Ni based electrodes suffer from a number of drawbacks: when utilizing natural gas fuel feeds, the catalytic activity of Ni can be reduced by formation of carbon or sulphur species on the active surface [1]. During long-term operation, agglomeration and microstructural change in the Ni phase is thought to drive performance degradation by reducing the active triple phase boundary available for reaction [2].

Ni based anodes also undergo significant dimensional change associated with the reduction/oxidation of Ni: reduction of NiO to Ni causes a volume change of -40.9% , while the reverse oxidation is associated with a volume change of $+69.2\%$ [3,4]. These anode microstructures must be carefully engineered in order to accommodate such significant microstructural evolution. Sarantaridis et al. provide an excellent review of the topic [3].

Because of the high temperature processing and sintering involved in electrode manufacture, Ni based electrodes are generally produced in NiO form with reduction to Ni occurring during first startup. During operation, the Ni phase will remain stable in a reducing environment, however re-oxidation can occur due to leakage or interruption to the fuel supply or due to increased pO_2 at high fuel utilizations [3].

During operation, nickel oxidation may occur under conditions of high fuel utilization and/or current density, or the anode may undergo oxidation due to failure of the fuel delivery system, or air leakage. Under these conditions the dimensional changes associated with oxidation are not necessarily reversible. During the course of numerous redox cycles, this can impact on the mechanical integrity, performance and lifetime of the electrode.

In recent years, the development of high-resolution tomography has provided a platform to explore SOFC electrode microstructures in three-dimensions and with unprecedented detail. Tomography techniques spanning a spectrum of spatial and temporal resolutions are now widely available to the materials engineer [5]. At length scales of relevance for SOFC electrode characterization, X-ray

* Corresponding author. Tel.: +44 207 679 3783.

E-mail address: p.shearing@ucl.ac.uk (P.R. Shearing).

techniques are uniquely flexible, allowing non-destructive imaging while accommodating a variety of thermal and gas environments.

Microstructural evolution processes are known to drive performance degradation in SOFC, however these processes remain poorly understood. Tomography techniques provide a platform for exploring microstructural changes associated with processing, operation and aging [6–8].

Owing to widespread availability, the most extensively adopted tomography technique utilizes the milling power of a focused ion beam (FIB) in conjunction with the imaging capabilities of high resolution FE-SEM, to provide a sequence of 2D images that can be effectively re-combined in 3D space. However, because this technique is destructive, studies of microstructural evolution are influenced by inherent sample variability. Non-destructive X-ray nano-computed tomography (CT) [9–11] provides a platform for exploring dynamic microstructural change in the absence of these possible complications and is compatible with both laboratory and synchrotron radiation. The authors have previously demonstrated a technique for preparation of optimal sample geometries for X-ray nano-CT [12], while this FIB sample preparation route will involve the selective removal of portions of the fuel cell electrode microstructure (and therefore *may* be destructive to the working fuel cell), the non-destructive X-ray characterization technique allows repeated, non-destructive characterization of the selected sample which facilitates the study of microstructural evolution processes in response to various environmental changes.

Here we present the application of high resolution, synchrotron nano-CT to study the dynamics of thermal oxidation of the Ni phase in a porous Ni–YSZ composite electrode exposed to high pO_2 at elevated temperatures.

2. Experimental

Fuel cell analogue microstructures have been manufactured to explore the effects of Ni oxidation on Ni–YSZ microstructures. NiO–YSZ powder (66 wt.% NiO, 34 wt.% YSZ) was purchased from Nextech Fuel Cell Materials, the powder was pressed into pellet form under 1000 kg load before sintering at 1350 °C for 12 h. The resulting pellets were reduced in H_2 at 900 °C for 4 h. This process results in samples with relatively large sintered particle size which facilitates technique development for tracking particle-by-particle microstructural evolution in these complex porous microstructures.

In order to provide an optimal geometry for fixed field of view (FOV) nano-CT, a focused ion beam (FIB) sample preparation technique has been used. The technique, which is described in more detail elsewhere [12], utilizes the nano-scale milling and manipulation capabilities of the FIB to prepare samples with a principal dimension matched to the microscope FOV, secured to a tungsten needle using a Pt micro-weld (see Fig. 1b).

Tomography experiments have been conducted using the Xradia nanoXCT-S100 transmission X-ray microscope (TXM) at beam-line 32-ID at the Advanced Photon Source, Argonne National Lab, IL, USA. This system utilizes X-ray optics to focus the beam before and after transmission, routinely achieving ca. 30 nm resolution in this facility. This can be coupled with the variable X-ray energy to perform multiple energy scans and X-ray absorption spectroscopy (XAS).

In order to capture the dynamic change associated with Ni oxidation, the sample prepared using the FIB lift-out techniques was subjected to the heating profile detailed in Fig. 1a. The sample was heated at a rate of 40 °C/min to the set point temperature and held for 10 min. The heating process was conducted in air, in a conventional laboratory furnace ex-situ of the microscope stage.

In total, 5 tomography sequences were collected at various stages during the oxidation process; scan A of the reduced sample as prepared, scans B to E following heating in air with hold temperature of 200, 300, 500 and 700 °C respectively.

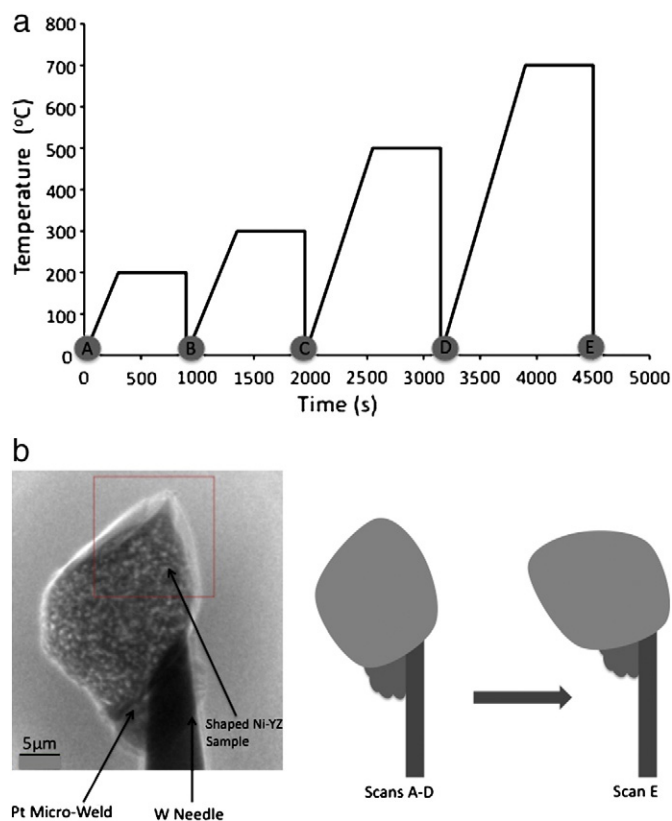


Fig. 1. a: Graph showing the ex-situ, in-air, heating profile used for step-wise oxidation of the Ni–YSZ composite b: A radiograph of a lift-out sample alongside a schematic illustrating the partial mechanical failure of the sample following a high temperature oxidation step.

In previous experiments using this system, the authors have demonstrated the ability to isolate triple phase contact in Ni–YSZ electrodes by conducting tomography above and below the characteristic Ni X-ray absorption edge [11]. In this work, the authors have conducted imaging at a single energy (8400 eV) just above the Ni edge, which provides sufficient contrast to identify each constituent phase (see Fig. 2). An additional calibration tomography sequence was also collected at 8.3 keV. For each tomography sequence (A–E), 360 images were collected at 0.5° increments across a 180° rotation with 8.4 keV X-ray illumination resulting in a 25 nm voxel size after reconstruction.

The transmission data was aligned relative to a fiducial marker and reconstructed using the Xradia XMReconstructor software. The resulting image sequences were segmented using a combination of median filtering in ImageJ [13] and an edge-preserving smoothing algorithm implemented in Avizo Fire (Visualization Sciences Group, Bordeaux, France).

During the final heating step some mechanical failure of the sample was observed. Fig. 1b shows a sample radiograph alongside a schematic diagram illustrating the change in sample geometry following the 700 °C heating step. The cause of this mechanical failure is not known and may be associated with manual handling, thermal shock, failure of the Pt micro-weld or as a result of the stresses generated during the high temperature oxidation. In other experiments the integrity of the Pt weld during rapid thermal cycling has been demonstrated [16], and the authors have found no chemical or morphological evidence suggesting diffusion of the Pt.

In spite of this loss of image registration between scan D and E, the sample was maintained within the microscope FOV for collection of the final tomography sequence E. Fig. 2 shows tomograms (2D virtual slices from 3D data sets) from scans A, C, D and E, showing the

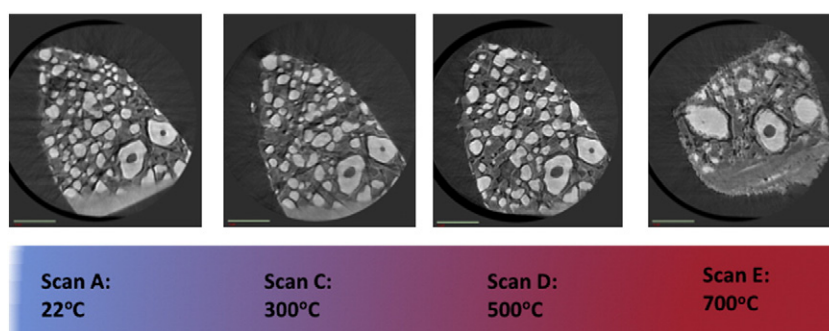


Fig. 2. Tomograms from 3D data sets collected at various points of the oxidation cycle, the Ni phase is shown in white, YSZ in gray with the surrounding pore phase in dark gray (Please note that owing to sample movement and resulting registration loss it is not possible to directly compare tomograms for scan E with lower temperature tomograms in this figure. The authors believe that small errors in image registration are responsible for the minor changes observed in tomograms for scans A–D).

microstructural evolution processes associated with step-wise oxidation of the Ni phase.

3. Results and discussion

Five tomography sequences were collected using the same imaging parameters following step-wise oxidation of the metallic Ni phase. Fig. 2 shows tomograms from various points in the oxidation profile. These 2D virtual slices demonstrate limited microstructural evolution occurring between scans A to D, as a result of heating the Ni in air following the heating profile indicated previously. Following the highest temperature (700 °C) oxidation step, significant evolution is observed as a result of Ni to NiO transition with observable densification and NiO film growth (Fig. 3).

This sequence of 2D dimensional tomograms reveals important information on the processing of the original Ni–YSZ microstructure – as illustrated in Figs. 2 and 3, there is evidence of a NiO core at the centre of large Ni grains, suggesting that in spite of the rigorous reduction conditions employed during processing, full reduction of the NiO phase was not achieved. The authors believe this is because of the high operating temperature employed during the reduction step of electrode processing: at low temperatures the rate of NiO oxidation is dictated by the kinetics of the reaction at the Ni/NiO interface [3]; however at higher temperatures, this process becomes distorted by Ni sintering which can restrict the access/egress of gas to the Ni/NiO interface [14]. The presence of an un-reduced NiO core in larger Ni grains (see Figs. 2 and 3) supports this high temperature mechanism.

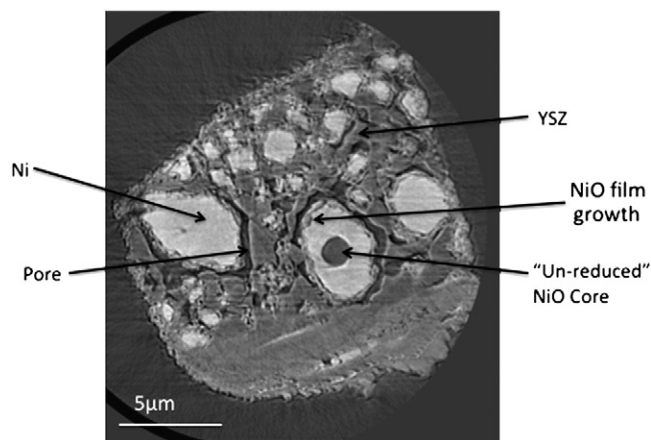


Fig. 3. A tomogram from scan E, conducted following high temperature oxidation, illustrating the phases present. The annotations show an un-reduced region in the center of a Ni particle and the growth of a NiO film following ex-situ oxidation.

Because of the limited evolution observed between scans A and D, two 3D renderings are presented, one for scan B and another for scan E. Fig. 4 shows the changing morphology of the Ni phase during the partial oxidation process.

The volumetric change associated with Ni oxidation is manifested as a loss of porosity; this densification is demonstrated in two dimensions in Figs. 2 and 3, and in three dimensions in Fig. 4. During this partial oxidation, the bulk porosity (measured for rendered sections of scans B and E) decreased from 23.1% to 15.5%.

Owing to the partial sample failure (between scans D and E) outlined previously, the rendered sections in Fig. 4a and b are not registered. The entire sample volume was maintained within the microscope FOV for the duration of all scans and material statistics have been extracted from the largest possible analysis volume for each scan to ensure fair comparison can be drawn between the samples B and E. A significant morphological change in the Ni phase is observed (Fig. 4) demonstrating a distinct microstructural evolution process.

In this experiment, the full FOV of the TXM was not utilized therefore providing analysis volumes between 325 and 844 μm^3 . In common with all tomography techniques a balance of sample volume and resolution must be achieved, to ensure sufficient resolution to characterize the sample features in a sample volume statistically representative of the bulk electrode. In order to ensure the boundary conditions for redox cycling in the microscopic sample were accurately re-created, microstructural analysis was conducted on the central portion of the sample. No spatial variation in the oxidation phenomena as a result of grain location within the sample has been observed.

The 3D reconstructions in Fig. 5 demonstrate the growth of a porous NiO film around the Ni particles, which effectively blocks the catalytically active surface and reduces the overall composite porosity. Coupled to the NiO film growth is a reduction in the Ni/pore interfacial area; the total Ni/pore interfacial area was reduced by 11.5 times upon oxidation, from 0.310 to 0.027 $\mu\text{m}^2/\mu\text{m}^3$ (normalized

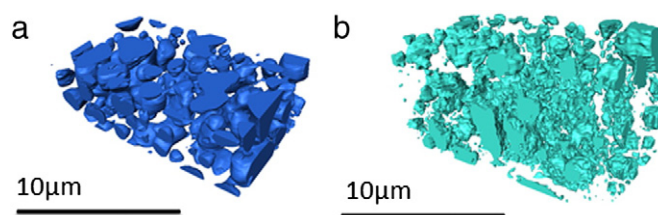


Fig. 4. a) Detail of rendering of the Ni phase from scan B following 200 °C air exposure (dimensions 7.08 × 12.68 × 3.63 μm). b) Detail of rendering of the Ni phase from scan E after 700 °C exposure (dimensions – 7.63 × 14.75 × 7.5 μm). NB – only the Ni phase is shown here, not NiO.

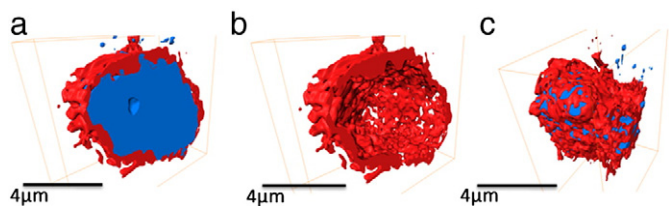


Fig. 5. Volume rendering from detail of scan E. a) 3D rendering showing the growth of a NiO film (red) on a Ni particle (blue) b) In the same orientation, the isolated NiO film shows internal porosity c) The same particle rotated shows blocking of the Ni surface by NiO and a decrease in the Ni/pore interfacial area.

for the different volumes of scans B and E as shown in Fig. 4). While it is unlikely that the fuel cell would be operational in the partially oxidized state the “blocking” effect of the NiO preventing oxygen access to the Ni phase will affect the continuing oxidation kinetics and also demonstrates the significant geometrical change associated with this process.

Upon oxidation, oxygen absorbing on the surface of a Ni particle will form a NiO film with a Ni core. Continued exposure to oxidizing conditions results in Ni transport from the particle core to the NiO/gas interface, which generates porosity in the NiO film (as shown in Fig. 5). Because of this porosity, the volume changes due to the Ni/NiO redox cycle are not reversible and can drive microstructural degradation.

For the particle shown in Fig. 5, (following heating to 700 °C) the average oxide layer thickness was found to be 502 nm although this varied from 0 nm (no layer) up to ca. ~1 μm but with most thicknesses <700 nm. The oxide layer structure is not homogenous across the Ni particle and these thickness variations in the film layer may affect local electrochemical performance.

In this experiment, limited microstructural change has been observed upon exposing the composite Ni–YSZ microstructure to temperatures up to 500 °C in air. The rate of oxidation will also be dependent on the local pO_2 within the structure (and therefore a function of the effective transport parameters and geometry of the structure itself). The microstructure examined here is relatively dense (compare e.g. with Iwai et al [15]) and therefore the transport limitation will be exacerbated: for these structures, however, short-term air exposure at 500 °C does not drive significant microstructural degradation. This may have implications for SOFC operating management, although clearly further investigation of technologically relevant electrodes is necessary to explore this in detail.

4. Conclusions

Volume changes associated with redox cycling of Ni based electrodes for SOFCs can drive significant microstructural degradation. This can result in degradation over time from nickel oxidation under conditions of high fuel utilization and/or current density or if the SOFC undergoes redox cycles during its lifetime from failure of the fuel delivery system, or due to air leakage.

The use of X-ray nano-CT has been demonstrated as a method for exploring changes in functional material microstructure, its non-

destructive nature enabling direct comparison of material microstructures before and after an environmental change. The technique has been used to explore the effects of step-wise oxidation of a Ni–YSZ composite anode, showing a change in Ni morphology, the overall densification of the composite microstructure and the growth of a porous NiO film in three dimensions.

Recently, the development and implementation of a heating stage for operation in-situ of the TXM stage has been demonstrated [16], providing the potential to track microstructural evolution processes associated with Ni oxidation without removal of the sample to an external furnace. Furthermore, combined with techniques for 3D X-ray absorption near edge spectroscopy (XANES) [17] there is significant potential to simultaneously monitor chemical and microstructural change in-situ using synchrotron nano-CT.

The application of these techniques is not limited to fuel cell research and may find application in a range of fields where microstructural evolution processes affect device or material lifetime, for example batteries, catalysts and structural ceramics.

Acknowledgements

The authors acknowledge the financial support from the EPSRC Supergen Fuel Cells programme and the EPSRC and University of Manchester funding for the establishment of the Henry Moseley X-ray Imaging Facility at Manchester. The support and expertise of Xradia and Visualization Sciences Group is also acknowledged.

The U.S. Department of Energy, Office of Science and Office of Basic Energy Sciences supported the use of the Advanced Photon Source at Argonne National Laboratory, under Contract no. DE-AC02-06CH11357. Data was collected at beam-line XOR 32-ID and the support of the instrument scientists is gratefully acknowledged.

Finally, the authors thank Prof. Alan Atkinson for useful discussions and insights.

References

- [1] G.J. Offer, J. Mermelstein, E. Brightman, N.P. Brandon, *J. Am. Ceram. Soc.* 92 (2009) 763–780.
- [2] A. Faes, A. Hessler-Wyser, D. Presvytes, C.G. Vayenas, J. Van Herle, *Fuel Cells* 9 (2009) 841–851.
- [3] D. Sarantaridis, A. Atkinson, *Fuel Cells* 7 (2007) 246–258.
- [4] D. Waldbillig, A. Wood, D.G. Ivey, *J. Electrochem. Soc.* 154 (2007) B133–B138.
- [5] P.R. Shearing, D.J.L. Brett, N.P. Brandon, *Int. Mater. Rev.* 55 (2010) 347–363.
- [6] J.S. Cronin, J.R. Wilson, S.A. Barnett, *J. Power Sources* 196 (2011) 2640–2643.
- [7] P.R. Shearing, PhD Thesis, Earth Science and Engineering, Imperial College, London, 2009.
- [8] H. Muroyama, H. Sumi, R. Kishida, J.Y. Kim, T. Matsui, K. Eguchi, *ECS Trans.* 35 (2011) 1379–1387.
- [9] K.N. Grew, Y.S. Chu, J. Yi, A.A. Peracchio, J.R. Izzo, Y. Hwu, F. De Carlo, W.K.S. Chiu, *J. Electrochem. Soc.* 157 (2010) B783–B792.
- [10] Y. Guan, W. Li, Y. Gong, G. Liu, X. Zhang, J. Chen, J. Gelb, W. Yun, Y. Xiong, Y. Tian, H. Wang, *J. Power Sources* 196 (2011) 1915–1919.
- [11] P.R. Shearing, J. Gelb, J. Yi, W.K. Lee, M. Drakopoulos, N.P. Brandon, *Electrochem. Commun.* 12 (2010) 1021–1024.
- [12] P.R. Shearing, J. Gelb, N.P. Brandon, *J. Eur. Ceram. Soc.* 30 (2010) 1809–1814.
- [13] W.S. Rasband, *ImageJ*, U. S. National Institutes of Health, Bethesda, Maryland, USA, 1997–2011.
- [14] T.A. Utigard, M. Wu, G. Plascencia, T. Marin, *Chem. Eng. Sci.* 60 (2005) 2061–2068.
- [15] H. Iwai, N. Shikazono, T. Matsui, H. Teshima, M. Kishimoto, R. Kishida, D. Hayashi, K. Matsuzaki, D. Kanno, M. Saito, H. Muroyama, K. Eguchi, N. Kasagi, H. Yoshida, *J. Power Sources* 195 (2010) 955–961.
- [16] P.R. Shearing, R. Bradley, J. Gelb, S.N. Lee, A. Atkinson, P.J. Withers, N.P. Brandon, *Electrochem. Solid-State Lett.* 14 (2011) B117.
- [17] G.J. Nelson, W.M. Harris, J.R. Izzo, K.N. Grew, W.K.S. Chiu, Y.S. Chu, J. Yi, J.C. Andrews, Y.J. Liu, P. Pianetta, *Appl. Phys. Lett.* 98 (2011).